Characterization of Enterovirus A71 entry factors in cell lines and Human Enteroids using CRISPR-Cas9 Knock-Out

Gasull-Celades, L.[1,2], García-Rodríguez, I.[1,2], Calitz, C.[1,2], Wolthers, K.C.[1] and Sridhar, A.[1,2]

1 - OrganoVIR Lab, Department of Medical Microbiology, Amsterdam UMC, Academic Medical Centre, University of Amsterdam, 1100 AZ Amsterdam, The Netherlands.
2 - Department of Pediatrics Infectious Diseases, Emma Children's Hospital, Amsterdam UMC, Academic Medical Centre, University of Amsterdam, 1100 AZ Amsterdam, The Netherlands.

Abstract. Enterovirus A71 (EV-A71), one of the main causative agents of hand, foot and mouth disease (HFMD), is a highly neurotoxic enterovirus belonging to the *Picornaviridae* family. EV-A71 results in outbreaks globally and is rising as a major public health concern. Despite its pathogenic potential, the entry pathway by which EV-A71 enters the host cell is still not fully understood. In this study, we characterized the role of two EV-A71 entry factors, SCARB2 and HSPG2, in cell lines and human intestinal organoids using CRISPR-Cas9 knock-out (KO) technology. Here, we show SCARB2 does not act as an entry receptor for EV-A71 as previously reported, since it is not involved in either binding nor internalization of viral particles. However, SCARB2 does play an essential role in later stages of EV-A71 infection, following internalization. Furthermore, HSPG2 is neither an entry receptor nor involved in EV-A71 infection in cell lines and human intestinal organoids. Our findings disprove the role of SCARB2 as an entry receptor and show HSPG2 as a non-essential factor for EV-A71 infection. This research further stresses the need to fully characterize the entry pathway of EV-A71, as the current understanding of viral pathogenesis is incomplete.

INTRODUCTION

Enterovirus A71 (EV-A71), a member of the *Picornaviridae* family, is a major public health concern due to recent global outbreaks[1–5]. EV-A71 is a non-enveloped, positive sense single-stranded RNA virus which can cause a wide variety of illnesses affecting multiple organs, such as the gastro-intestinal and respiratory tract[6–8]. In addition to being one of the leading causes of hand, foot and mouth disease (HFMD)[5], EV-A71 can also infect the central nervous system (CNS)[9,10]. EV-A71 CNS infection can lead to acute and life-threatening meningitis or encephalitis in young children, and it is now considered the primary cause of acute flaccid paralysis[11]. Due to this, the World Health Organization (WHO) has named EV-A71 as the most severe neurotoxic enterovirus[12]. Despite the high pathogenic potential of EV-A71, the aetiology of disease progression remains elusive. Elucidating viral host entry mechanisms in the primary entry site, the gastrointestinal tract[13], is a crucial step towards counteracting EV-A71 infection. However, current knowledge on how EV-A71 enters a host cell to initiate infection is inconclusive.

Multiple entry receptors for EV-A71 have been identified over the years. The most accepted, and recognized host factor is scavenger receptor class B member 2 (SCARB2)[14,15]. SCARB2 is a transmembrane protein, belonging to the CD36 family of scavenger receptors, the primary role of which is the reorganization and regulation of endosomal/lysosomal transport[16,17]. Multiple studies have demonstrated an essential role for SCARB2 in viral uncoating[18,19], a crucial step in EV-A71 infection. In addition, other studies indicate SCARB2 may play a pivotal role in EV-A71 attachment to the cell membrane, as well as internalization[20,21]. However, SCARB2 is primarily localised in the lysosomal membrane with low expression at the cell surface[16].Therefore, the role of SCARB2 as the primary entry receptor for EV-A71 is counterintuitive. Subsequently, other receptors have been identified to play a role in EV-A71 infection, such as heparan sulphate proteoglycans (HSPGs)[22], human P-selection glycoprotein ligand-1 (PSGL-1)[23] and annexin II (Anx2)[24], among others. HSPG2, in particular, is highly expressed in the gastrointestinal tract[25,26] and could act as an attachment receptor

supporting viral binding to the cell surface and internalization[27] followed by SCARB2-dependent uncoating in the endolysosome.

The aforementioned studies on EV-A71 entry have been performed in immortalized cell lines, which present several crucial limitations. First, cell lines do not accurately represent the human in vivo condition, since most are tumour or animal-derived, and are functionally aberrant[28,29]. Furthermore, cell lines are oversimplified models of the otherwise highly complex system and structure of human tissues, which can strongly influence viral entry[30]. For instance, a study found EV-A71 to predominantly infect via the basolateral side of a primary intestinal model, demonstrating the importance of maintaining tissue-specific structures for viral infection studies[31]. Second, serial passaging of cell lines for long periods of time leads to the development of genomic alterations and clonal variation[32]. Consequently, studies performed in the same cell lines can present contradictory or non-reproducible results between laboratories or even within the same lab[33]. Therefore, the translational relevance of immortalized cell lines as models of the multifactorial in vivo viral-host interactions, is questionable.

To overcome these limitations, human organoids are promising tools that have been suggested to have better translation in vivo[34]. Organoids are stem-cell derived 3D constructs, which can replicate the functionality and cellular architecture of human organs[35]. These models can recreate the complexity found in human tissues needed to fully uncover the authentic virus-host interactions, providing an ideal platform for viral infection studies. For instance, human enteroids present cell heterogeneity, being composed of: Paneth cells, enterocytes, enteroendocrine cells, goblet cells and stem cells, all of which are present in the in vivo human tissue[36]. This property, not only recreates the physiological cell-cell interactions that viruses naturally encounter, but it also allows viral tropism studies[37].

Therefore, in this study, we aim to further elucidate the role of SCARB2 and HSPG2 in EV-A71 infection using a more physiologically relevant model, human intestinal organoids models, as well as cell lines. To this end, we utilized CRISPR-Cas9 technology to knock-out the expression of SCARB2 and HSPG2 in the mentioned models and challenged them with EV-A71 to characterize viral entry.

MATERIALS AND METHODS:

Cell and Virus Culture

RD99 cells (human rhabdomyosarcoma cells, provided by the Dutch National Institute for Public Health and the Environment (RIVM), were cultured in Eagle's minimum essential medium (EMEM, Gibco, 32360-026) containing 8% (v/v) heat-inactivated fetal bovine serum (FBS, Lonza, 15B008), 1% (v/v) Non-essential amino acids (100x, ScienceCell Research Laboratories, 0823), 0.1% (v/v) L-glutamine (Lonza, BEBP17-605E) and 100 U/mL of penicillin and streptomycin (Pen/Strep, Thermo Fisher Scientific, 15140-122). Cells were incubated at 37°C, 5% CO_2 and passaged weekly. For passaging, cells were washed with Phosphate Buffered Saline (PBS, Lonza, 15140-122) and incubated for 5 minutes in Trypsin-EDTA 0.05% (Gibco, 25306-054) at 37°C, 5% CO_2 to obtain a cell suspension.

EV-A71 strain (C1-91-480, AB552982) was obtained from RIVM, Bilthoven and cultured on RD99 cells. EV-A71 virus stocks were aliquoted and stored at -80°C until further use. The Reed-Muench method[38] was used to determine the 50% tissue culture infective dose ($TCID_{50}$) of the viral stocks.

Human Intestinal Enteroid (HIE) Isolation and Culture

Enteroids were isolated following the protocol described previously[39]. Enteroids were passaged when Matrigel® (Corning, 356231) droplets were 80% confluent. Briefly, old media was removed and new ice cold Advanced DMEM/F12 (Thermo Fisher Scientific, 12634-028) supplemented with 7.5mM

HEPES (Sigma-Aldrich, H3375), 100 U/mL Pen-Strep (Thermo Fisher Scientific, 15140-122) and 0.5x Glutamax (Thermo Fisher Scientific, 35050-038), now referred to as Advanced DMEM/F12 +++, was added to dissolve the Matrigel®. Enteroids were collected in a tube and spun-down at 200 rcf for 5 minutes at 4°C. The pellet was washed with Advanced DMEM/F12 +++ and centrifuged again as previously described. Matrigel® was then added to resuspend the pellet and three droplets of 10 µL each were plated in a 24-well plate. Droplets were incubated at 37°C for 5-10 minutes, after which fresh IntestiCult® OGM Medium (STEMCELL Technologies, 100-0190), supplemented with IntestiCult® organoid supplement (STEMCELL Technologies, 100-0190) was added.

Human Intestinal Enteroid (HIE) 2D Culture in Transwell® inserts

The apical chamber of 0.4 µm Transwell® inserts (VWR, 734-3263) was pre-coated with a human laminin suspension containing 10 µg/cm^2 LN511 (LN, BioLamina, LN511-0502) and 5 µg/cm^2 LN521 (LN, BioLamina, LN521-05), for 2 hours at 37°C in a 24-well plate. After incubation and before seeding of enteroids, the laminin suspension was removed. Enteroids were collected in cold Advanced DMEM/F12 +++ and centrifuged at 200 rcf for 5 minutes at 4°C to remove Matrigel®. The pellet was washed again with Advanced DMEM/F12 +++. 1x TrypLE (Gibco, 12605-010) was added and incubated for 10 minutes at 37°C to generate a single cell suspension. Advanced DMEM/F12 +++ containing 15% (v/v) FBS was then added to inactivate the TrypLE and the cell suspension was centrifuged at 300 rcf for 5 minutes at 4°C. The pellet was resuspended in IntestiCult® Organoid Differentiation Medium (IntestiCult® ODMh, STEMCELL Technologies, 100-0214) supplemented with 10 µM Y-27632 Rho-kinase inhibitor (ROCK inhibitor, Sigma-Aldrich, Y0503). Cells were then counted and 100.000 cells/well were seeded in the apical chamber. 200 µL of IntestiCult® ODMh containing ROCK inhibitor was added to the apical side and 600 µL to the basolateral chamber. The monolayer was then incubated at 37°C, 5% CO_2. After 3 days, the media was changed to IntestiCult® ODMh and media was refreshed every day. After a confluent monolayer was formed, the plate was incubated at 37°C, 5% CO_2 on an orbital shaker at 65 rpm and media was refreshed every second day on the basolateral chamber but every day for the apical chamber. After 14 days, HIE monolayer with a trans epithelial electrical resistance (TEER) greater than 200 Ω·cm^2 were used for further experiments.

sgRNA Lentiviral Transduction for CRIPR-Cas9 Knock-outs

RD99 Transduction

Cas9 expressing RD99 cells (RD99 Cas9) were generated using Invitrogen™ LentiArray™ Cas9 Lentivirus (Thermo Fisher Scientific, A32064) according to the manufacturer's protocol. RD99 Cas9 cells were transduced with Invitrogen™ LentiArray™ CRISPR lentivirus particles carrying a sgRNA sequence (**Table 1**) targeting the desired genes, *SCARB2* and *HSPG2* (Thermo Fisher Scientific, A32042). Cas9 expressing cells were also transduced with Invitrogen™ LentiArray™ CRISPR Control Lentivirus (Thermo Fisher Scientific, A32060) as a positive control of transduction (**Figure 1**). The manufacturer's protocol was followed. Briefly, RD99 Cas9 cells were seeded in EMEM with 8% (v/v) FBS. Once the cells were 80% confluent, media was changed to EMEM with 2% (v/v) FBS containing 7 µg/mL Polybrene (Sigma-Aldrich, TR-1003) to enhance transduction. Then, the corresponding amount of Invitrogen™ LentiArray™ CRISPR lentiviral particles to obtain a multiplicity of infection (MOI) of 0.1, were inoculated and the plate was incubated at 37°C, 5% CO_2 overnight. Media was changed the following day to EMEM with 8% (v/v) FBS and incubated at 37°C, 5% CO_2. Transduced cells were then treated with 5 µg/mL of Puromycin (InvivoGen, #ant-pr-1) until all non-transduced cells died, after which transduced cells were cultured using EMEM with 8% (v/v) FBS media.

Table 1. sgRNA sequences targeting *SCARB2* and *HSPG2* genes.

Gene	sgRNA sequence
SCARB2	AATCCAGAGGAGATCCTCAG
HSPG2	ATCGTATGCCCTCAGCCCAT

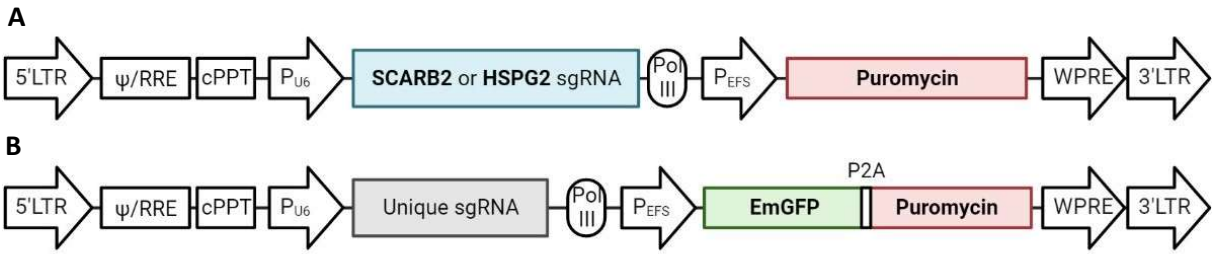

Figure 1. Invitrogen™ LentiArray™ CRISPR sgRNA lentiviral particles map **(A)** Map of the designed sgRNAs **(B)** Map of the control lentiviral particles carrying GFP. Created in Biorender.com

Expansion of a Single RD99 Clone

Transduced RD99 cells were collected using Trypsin-EDTA 0.05% (v/v) (Gibco, 25306-054) treatment and diluted in EMEM with 8% (v/v) FBS to a concentration of 10 cells/mL. 100 µL of cell suspension was added to all wells of a 96-well plate to obtain a desired concentration of 1 cell/well. Media was changed every 3-4 days. All clone colonies obtained were then collected and plated in 6-well plates for expansion. Media was changed every 3-4 days.

Enteroid Transduction

In addition to the Invitrogen™ LentiArray™ CRISPR lentivirus particles described above (SCARB2 sgRNA, HSPG2 sgRNA, and GFP Control), Invitrogen™ LentiArray™ Cas9 Lentivirus (Thermo Fisher Scientific, A32064) was simultaneously transduced in enteroids. Briefly, cultured enteroids were collected in Advanced DMEM/F12 +++ and centrifuged at 900 rcf for 5 minutes. The pellet was then resuspended in TrypLE to fragment the enteroids, and incubated at 37°C for 5 minutes until fragments of 5-10 cells were observed. Advanced DMEM/F12 +++ containing 10% (v/v) FBS was added to inactivate TrypLE and centrifuged again at 900 rcf for 5 minutes. Enteroids were then resuspended in IntestiCult OGMh media, supplemented with 10 µM ROCK Inhibitor and 8 µg/mL Polybrene (Sigma-Aldrich, TR-1003), containing the Invitrogen™ LentiArray™ CRISPR sgRNA and Cas9 lentiviral particles at a 1:5 ratio. The inoculated enteroids were seeded on a plate and centrifuged at 600 rcf for 1 hour at 32°C, followed by an incubation at 37°C, CO_2 for 6 hours. After incubation, the fragmented enteroids were collected, centrifuged at 900 rcf for 5 minutes and resuspended in Matrigel®. Three Matrigel® droplets were seeded and incubated at 37°C for 10-15 minutes and IntestiCult OGMh media added. After 2-3 days 1 µg/mL Puromycin (InvivoGen, #ant-pr-1) was added to select transduced enteroids. Media was changed after 2-3 days.

Single Enteroid Culture

Transduced enteroid cultures were observed over a light source and individual organoids were distinguished by eye. Using cut 200 µL tips, single organoids were collected in 1.5 mL tubes and Advanced DMEM/F12 +++ added. Tubes were centrifuged at 600 rcf for 10 minutes and the pellet was resuspended in 30 µL of Matrigel® (Corning). A single droplet of 30 µL was plated in a 24-well plate and incubated at 37°C for 10 minutes, after which IntestiCult OGMh media (STEMCELL Technologies,

100-0190) containing 10 µM ROCK-Inhibitor (Sigma-Aldrich, Y0503) was added. Once the single enteroid grew large enough to break into smaller pieces, enteroids were collected and passaged with TrypLE (Gibco, 12605-010) treatment, as previously explained, to obtain multiple enteroids derived from a single one. Media was changed every 2-3 days.

IBIDI Immunostaining and EV-A71 infection assays on RD99 cells

IBIDI® 8 well chamber, removable glass slides (IBIDI, 80841) were pre-coated with a human laminin suspension containing 10 µg/cm^2 LN511 (BioLamina, LN511-0502) and 5 µg/cm^2 LN521 (BioLamina, LN521-05), for 30 min to 1 hour at 37°C. Laminin suspension was removed and 100.000 RD99 cells per well was seeded in EMEM with 8% (v/v) FBS media, which were incubated overnight at 37°C with 5% CO_2. The following day, EMEM with 8% (v/v) FBS was removed and the EV-A71 dilution in EMEM with 2% (v/v) FBS with the corresponding MOI of 0.1 (replication assay) or 5 (binding and internalization assay) was added. For the replication assay, cells were incubated with virus for 2 hours at 37°C with 5% CO_2, after which the cells were washed with EMEM containing 2% (v/v) FBS and incubated overnight at 37°C with 5% CO_2. After incubation, cells were washed three times with PBS (Lonza, 15140-122) and fixed for 30 minutes at room temperature with 4% paraformaldehyde in PBS (PFA, Sigma-Aldrich, 252549-500ML). For the binding and internalization assay, after viral inoculation, cells were incubated for 1 hour at 4°C. Cells were then washed with PBS three times and for the binding assay, cells were fixed as previously described. For the internalization assay, after washing cells were incubated in EMEM with 2% (v/v) FBS for 1 hour at 37°C with 5% CO_2. Then, cells were washed again three times with PBS and fixed.

Once fixed, cells were permeabilized with ice-cold 100% Methanol for 5 minutes at room temperature. Then, cells were blocked using SEA BLOCK blocking buffer (SEA Block, Thermo Fisher Scientific, 37527) for 1 hour at room temperature. SEA BLOCK blocking buffer was then removed and 200 µL of corresponding primary antibody dilution in SEA BLOCK blocking buffer was added and incubated at room temperature for 2 hours. After incubation, the wells were washed three times with PBS containing 1% (v/v) Tween 20 (TBS, EMD Millipore, 524750) and 200 µL secondary antibody dilution SEA BLOCK blocking buffer was added and incubated for 1 hour at room temperature. Finally, secondary antibody was removed by washing three times with PBS and covered with ProLong™ Glass Antifade Mountant (Invitrogen, P36984) to place coverslips. Cells were imaged using the EVOS® FL cell imaging system (Thermo Fisher Scientific) and images were processed with the program ImageJ 1.50i for Windows. The antibodies used can be found in **Table 2**.

Table 2. List of antibodies and dyes used for immunofluorescence staining.

Target	Host	Company	Catalogue #	Dilution
Anti-hSCARB2/LIMPII	Rabbit	Abcam	ab176317	1:50
Anti-Enterovirus 71	Mouse	Sigma-Aldrich	MAB979	1:250
Hoechst 33342	-	Thermo Fisher Scientific	H3570	1:1000
Anti-Rabbit ALEXA488	Goat	Thermo Fisher Scientific	A21058	1:500
Anti-Mouse ALEXA680	Donkey	Thermo Fisher Scientific	A21206	1:500

DNA Isolation

ISOLATE II Genomic DNA isolation Kit (BIOLINE) was used for DNA Isolation and the manufacturer's protocol was followed. RD99 cells from a confluent 6-well plate were washed with PBS (Lonza, 15140-122) and buffer GL was added. To detach the cells, the plates were frozen and after 5 minutes the surface of the plate was scratched with a pipette tip, allowing collection of cell suspension. For enteroid DNA Isolation, enteroids were collected and washed twice with PBS (Lonza, 15140-122) to

remove Matrigel® before DNA Isolation. Isolated DNA was measured using NanoDrop™ 2000 (Thermo Fisher Scientific), using Buffer G from the ISOLATE II Genomic DNA Kit as a blank control.

Protein Isolation

Both RD99 and enteroids were washed twice with PBS before protein isolation. Cells were collected by adding NP40 buffer (Thermo Fisher Scientific, J60766.AP) containing 25x protease Inhibitor Cocktail (Calbiochem, 539137) and pipetting up and down to lyse the cells. Lysed cells were then centrifuged at 350 rcf for 20 minutes at 4°C and the supernatant was collected. Pierce™ BCA Protein Assay Kit (Thermo Fisher Scientific, 23225) was used as described by the manufacturer to quantify protein concentration.

PCR and Sequencing

Isolated DNA was amplified using the FastStart™ Taq DNA polymerase kit (Sigma-Aldrich, 12032929001) following the manufacturer's instructions. The primers used for each gene can be found in **Table 3**. The PCR thermal cycle used is the following: initial denaturation was programmed for 5 min at 95°C, followed by 45 cycles of 30s at 95°C of denaturation, 30s at 59°C as the annealing temperature, and 1min at 72°C for extension. Finally, for the final extension, 10 min at 72°C were programmed. For sequencing, PCR products were purified using PureLink™ Quick Gel extraction Kit (Invitrogen, K210012) following the manufacturer's protocol. Then, 5 µL of DNA samples and 5 µL of 20 µM Forward primers were combined and sequenced using Sanger sequencing technology by Macrogen Europe.

Table 3. Sequence of all primers utilized for PCR amplification of *SCARB2* and *HSPG2*. Tm: Melting Temperature.

Gene	Primer	Sequence	Tm (°C)
hSCARB2	Forward	5'- TTCTTTCAAGACAGGAGGTGGT -3'	60.1
	Reverse	5'- CAAATGCCTCAGTACCATTCCT -3'	60.4
hHSPG2	Forward	5'- CAGAAAGGTACGAATGTGTCCA -3'	60.0
	Reverse	5'- TTTTGATTCAGTTTCCCCAAGT -3'	59.9

Western-Blot

Isolated proteins were diluted in 2x Laemmli buffer (BioRad, 1610737) with β-mercaptoethanol, heated at 99°C for 5-10 minutes and cooled down on ice. Pre-cast gel (Mini-PROTEAN TGX Stain-free gels 7.5%, BioRad, 4568023) was mounted and put in running buffer, made from diluting 10x Tris/Glycine/SDS buffer (Biorad, 1610732) in distilled water. Samples and ladder (Precision Plus Protein™ Dual Xtra Prestained Protein Standards, BioRad, 1610377) were then loaded onto the gel and run at 120V for 60-90 minutes at 4°C. The gel was then mounted in a transfer sandwich containing PVDF membranes, filter paper and sponges, all soaked in 1x transfer Buffer (10x Tris/Glycine buffer, Methanol and distilled water) and run for 50 minutes at 25V at 25°C. The PVF membrane with the transferred proteins was then soaked in blocking solution for 30 minutes, which contains 5% (w/v) milk in PBS-T (PBS with 0.1% Tween-20, EMD Millipore, 524750). Then, the membrane was cut in half by the 65 kDa mark and incubated in blocking solution containing the corresponding primary antibody overnight on a shaker at 4°C. The membrane was then washed with PBS-T multiple times for 5 minutes and incubated for 2 hours in blocking solution containing the corresponding secondary antibodies conjugated with horseradish peroxidase (HRP). The membranes were washed again in PBS-T for 45 minutes and incubated in Clarity™ Western ECL substrate (BioRad, 1705060). The membrane was the imaged using Image Quant LAS4000. The antibodies utilized can be found in **Table 4**.

Table 4. List of antibodies used for Western-Blot.

Target	Host	Company	Catalogue #	Dilution
Anti-hSCARB2/LIMP2	Goat	Sigma-Aldrich	SAB2501242	1:1000
Anti-HSPG2/Perlecan	Mouse	Thermo Fisher Scientific	13-4400	1:500
Anti-β-Tubulin	Mouse	Thermo Fisher Scientific	MAS-16308	1:2000
Anti-Mouse IgG (H + L)-HRP Conjugate	Goat	BioRad	1706516	1:3000
Anti-Goat IgG, HRP	Donkey	Promega	V8051	1:3000

EV-A71 Infection of RD99 cells

RD99 cells were infected with EV-A71 at MOI of 0.1 and 1. $TCID_{50}$ assay on RD99 cells was used to quantify infectious particles for MOI calculations. Viral dilutions were prepared in EMEM with 2% (v/v) FBS and added to RD99 cells for 1 hour at 4°C. After incubation, cells were washed three times with EMEM with 2% (v/v) to remove unbound virus particles and incubated for 10 minutes at 37°C with 5% CO_2, after which the 0h time-point supernatant sample was collected. To do so, 100 µL of supernatant was removed and fresh 100 µL of EMEM with 2% (v/v) FBS added. Supernatant samples were collected at 2, 8, 12 and 24h post infection.

EV-A71 Infection of Enteroid monolayers

Isolated crypts from a 19-week fetal donor were used for Transwell® enteroid monolayer cultures and infected with EV-A71 at a MOI of 1. 100 µL of the viral dilution was added to the basolateral side and incubated at 4°C for 1 hour. Following incubation, both the apical and basolateral sides were washed three times with IntestiCult® ODMh (STEMCELL Technologies, 100-0214) and incubated at 37°C with 5% CO_2 for 10 minutes, after which 100 µL of supernatant was collected from the apical and basolateral side for the 0h time-point. 100 µL of medium were replenished and media was collected from both the apical and basolateral compartments at: 24, 48 and 72h post infection.

EV-A71 Binding and Internalization assays

For both the binding and internalization assays, cells were infected with EV-A71 as previously described for RD99 and enteroid monolayers. For the binding assay, after incubation with the viral dilution at 4°C for 1 hour, the medium was removed and washed three times with PBS (Lonza, 15140-122) to remove unbound viral particles. 300 µL of Lysis Buffer (PureLink™ RNA Mini kit, Thermo Fisher Scientific, 12183025) was then added to each well and cooled at -20°C for 3-5 minutes to facilitate cell harvesting. Samples were stored at -80°C for future RNA Isolation procedure. The same procedure was followed for RD99 cells and enteroid monolayer cultures. For the internalization assay, upon incubation at 4°C for 1 hour with the virus, cells were washed three times with EMEM containing 2% FBS or IntestiCult ODMh, for RD99 cells and enteroid monolayers respectively, to remove unbound viral particles. Then, infected cell cultures were incubated for an additional hour at 37°C with 5% CO_2. After incubation, 500 µL of Trypsin-EDTA 0.05% (v/v) (Gibco, 25306-054) was added to detach and collect cell suspension, as well as to remove membrane bound viral particles. Cell suspension was centrifuged at 600 rcf for 4 minutes, the supernatant of which was removed, and the pellet washed three times with PBS (Lonza). Finally, the cell pellet was resuspended in 300 µL of Lysis Buffer (PureLink™ RNA Mini kit, Thermo Fisher Scientific, 12183025) and stored at -80°C until further use.

RNA Isolation and cDNA synthesis

Viral RNA was isolated from 25 µL of supernatant samples using PureLink™ RNA Mini kit (Thermo Fisher Scientific) according to the manufacturer's instructions. From the eluted RNA, 40 µL was reverse-transcribed into cDNA, by adding 10 L of a Superscript™ II reverse transcriptase (Thermo Fisher) Mastermix and incubating at 42°C in a shaker at 350 rpm for 30 minutes. cDNA was stored at 4°C.

Quantitative real-time PCR (RT-qPCR)

SYBR™ Green PCR Master Mix (Thermo Fisher Scientific, 4309155) containing primers targeting the 5'UTR region of EV-A71 genome was used. The primers used were the following: Forward: 5'-GGCCCTGAATGCGGCTAAT-3' Reverse: 5'-GGGATTGTCACCATAAGCAGCC-3'. The aforementioned PCR Master Mix combined with cDNA samples were run for qPCR using CFX Connect Real-Time PCR detection System (Bio-Rad, California, USA). Viral RNA copy numbers were obtained through the conversion of Cq values against a standard curve with known viral genome concentrations.

Statistical analysis

GraphPad Prism version 9.5.1 for Windows (GraphPad Software Inc., La Jolla, USA) was used for the statistical analysis of all experimental data analysed. Statistically significant differences were assessed using two-way ANOVA analysis to compare between groups. Only P values lower than 0.05 were considered statistically significant, with *P<0.05, **P<0.01, ***P<0.001 and ****P<0.0001. Standard error of mean (SEM) is represented by bars.

RESULTS

Generation and validation of SCARB2 knock-out clonal populations in RD99 and enteroids

In order to characterize the role of SCARB2 as a potential entry receptor for EV-A71, SCARB2^{KO} lines were generated in both RD99 cells and enteroids using CRISPR-Cas9 technology. Briefly, RD99 and enteroid cells were transduced with the lentiviral particles carrying the corresponding sgRNA sequences (see materials and methods). The lentiviral sgRNA constructs carry a puromycin selection marker which allowed for the selection of successfully transduced cells. To ensure pure KO populations of the target genes, single RD99 cells and single enteroid clones were generated and expanded. Each clonal population was then validated for successful KO either by sequencing, to identify potential indels (nucleotide insertions or deletions), or by western blot or immunostaining, ensuring loss of expression of the target proteins (**Figure 2A**).

To validate the KO of SCARB2, the protein expression in the RD99 and enteroid SCARB2^{KO} clones was assessed by western blotting. The SCARB2^{KO} RD99 clonal population showed no expression of SCARB2 when compared to RD99-WT, indicating that a successful pure KO population was obtained (**Figure 2B**). A faint band can be observed in the enteroid-SCARB2^{KO} clonal population, however, SCARB2 expression is highly diminished when compared to the enteroid-WT (**Figure 2C**). This suggest that the enteroid-SCARB2^{KO} population obtained was successfully knocked out, although a small percentage of WT cells may remain. To further validate loss of SCARB2 protein expression, we performed an immunostaining on RD99-WT and RD99-SCARB2^{KO} cells. No expression of SCARB2 was detected in the RD99-SCARB2^{KO} clonal population, while in RD99-WT, expression of SCARB2 was clearly observed (**Figure 2D**). Thus, KO clonal populations of SCARB2 were successfully obtained and validated in both RD99 cells and enteroids through the loss of protein expression.

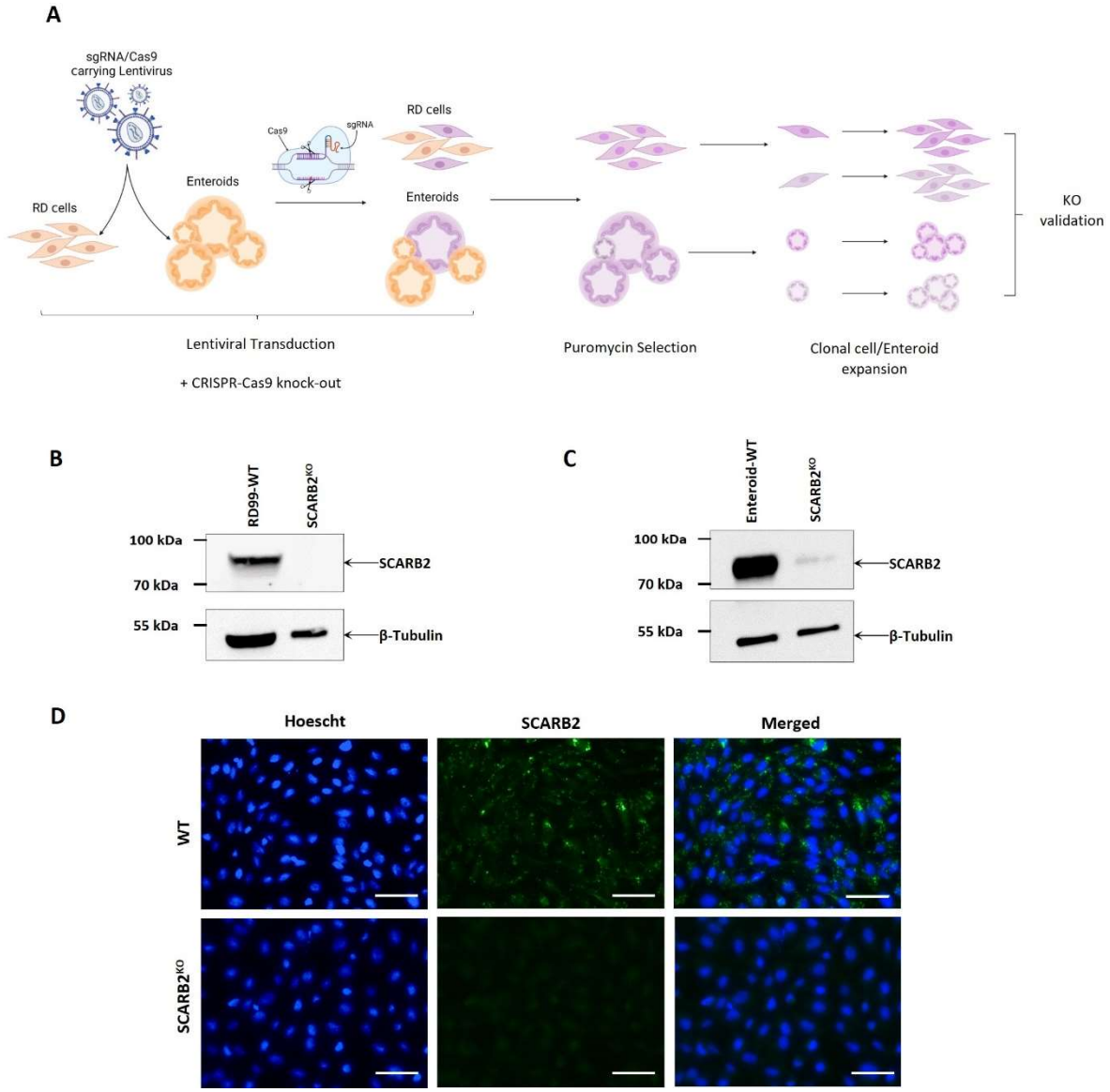

Figure 2. Obtention of successful SCARB2 KO in RD99 and enteroid clonal populations. (A) Schematic representation of the experimental set-up utilized for the generation and validation of CRISPR-Cas9 KO lines (Created in Biorender.com **(B and C)** Western blot results of SCARB2 protein expression in WT and SCARB2^{KO} clones of RD99 and Enteroids, respectively. **(D)** IBIDI Immunostaining of RD99-WT and RD99-SCARB2^{KO} cells. Cultures were stained with Hoechst (blue) and anti-hSCARB2 antibody (green). Scale bars in white represent 50µm.

SCARB2 is essential for EV-A71 infection in RD99 cells as well as in enteroids

Once a pure RD99 and enteroid populations with SCARB2^{KO} were obtained, they were challenged with EV-A71 to characterize the importance of SCARB2 for infection. As shown in **Figure 3A**, RD99-WT cells showed increasing levels of cytopathic effect (CPE) after 24 hours correlated with the MOI used. Contrarily, RD99-SCARB2^{KO} presented no or minimal CPE regardless of the MOI used. This suggests that the absence of SCARB2 greatly hindered the cytopathic effect induced by EV-A71, and hence, knocking-out SCARB2 conferred resistance to EV-A71 infection.

To further confirm the lack of infection in SCARB2^{KO} cells upon EV-A71 inoculation, the number of viral copies present in the supernatant after 24 hours was quantified by RT-qPCR. RD99-SCARB2^{KO} resulted in a significant reduction in viral copy numbers at both MOI of 0.1 and 1 when compared to RD99-WT, which showed a 100-fold increase in viral copy numbers (**Figure 3B**). These results suggest that SCARB2

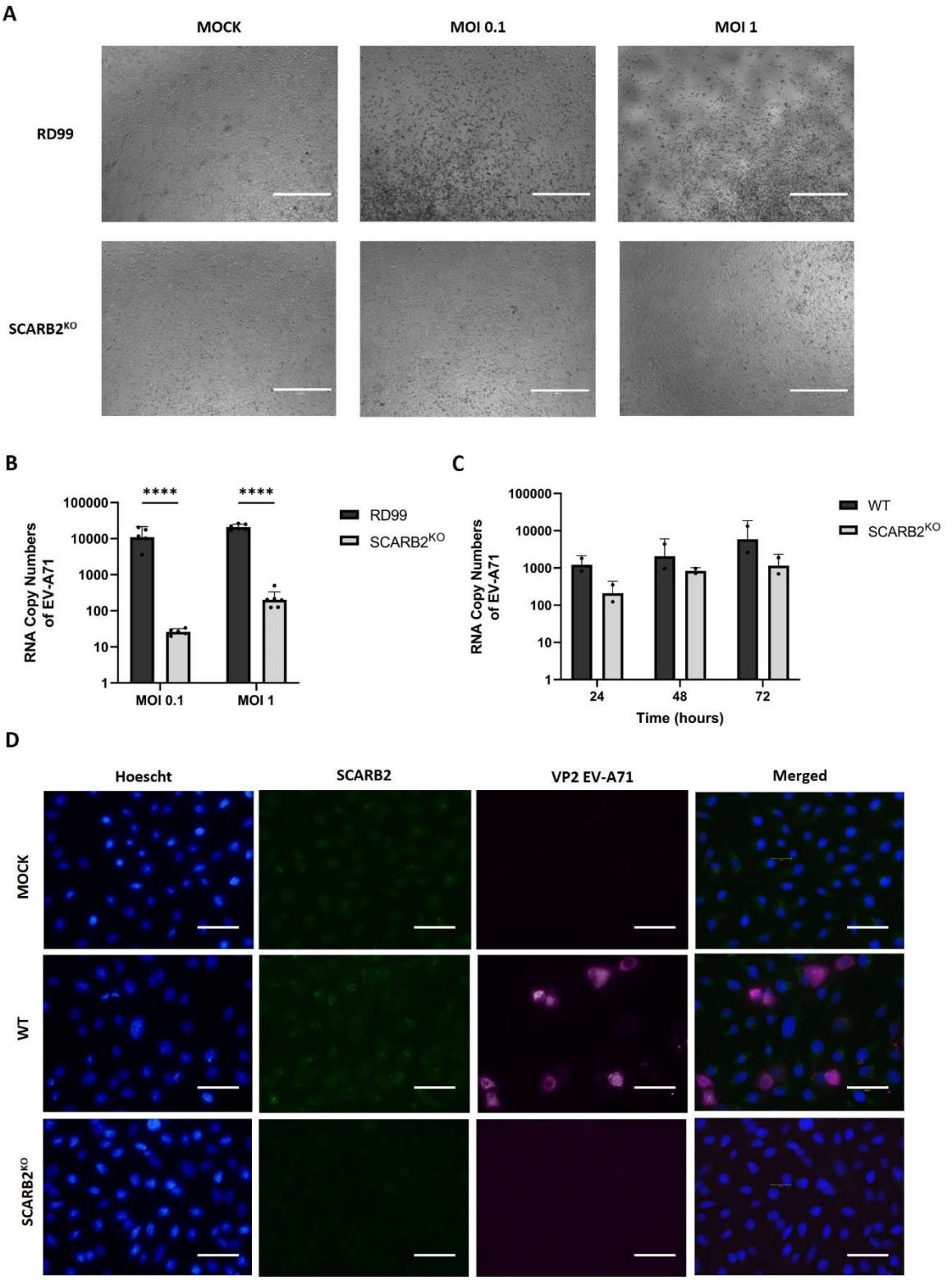

Figure 3. Absence of SCARB2 expression hinders EV-A71 infectivity in RD99 and enteroids (A) Bright field images depicting cytopathic effect (CPE) induced by EV-A71 infection of RD99-WT and RD99-SCARB2^{KO} using MOI of 0.1 and 1. Scale bars in white represent 750 µm. **(B)** Viral RNA copy numbers of EV-A71 in RD99-WT and RD99-SCARB2^{KO} supernatant samples after 24h of EV-A71 infection. **(C)** Viral RNA copy numbers of EV-A71 in enteroid-WT and enteroid-SCARB2^{KO} supernatant samples collected from the apical compartment of Transwell® inserts at 24-, 48- and 72-hours post infection. Transwell® cultures were infected with an MOI of 1 from the basolateral compartment **(D)** IBIDI immunostaining analysis of RD99-WT and RD99-SCARB2^{KO} infected with EV-A71 with an MOI of 0.1 for 24 hours. MOCK refers to RD99-WT. Cultures were stained with Hoechst (blue), anti-hSCARB2 antibody (green) and anti-VP2-EVA71 (magenta). Scale bars in white represent 50 µm.

is essential for EV-A71 replication in RD99 cells, and its absence significantly hinders CPE and viral replication.

Furthermore, we corroborated these findings with an immunostaining assay visualising the effect of SCARB2^{KO} on EV-A71 infection. As expected, no viral particles are present in the SCARB2^{KO} condition when compared to the WT conditions, in which strong EV-A71 signal is present (**Figure 3D**). These results further confirm the generation of a successful SCARB2^{KO} clonal population and consolidates SCARB2 as an essential host factor for EV-A71 infection.

Next, Transwell® enteroid-WT and enteroid-SCARB2^{KO} cultures were challenged with EV-A71. Viral particles were inoculated on the basolateral compartment and samples for RT-qPCR were collected from the apical compartment, since EV-A71 has been previously shown to infect basolaterally and shed apically[31]. As shown in **Figure 3C**, the SCARB2^{KO} conditions resulted in a slight reduction in EV-A71 viral copy numbers at all time-points analysed when compared to the WT condition. However, the reduction in viral copy numbers due to SCARB2^{KO} in the enteroids was not comparable to RD99-SCARB2^{KO}. Thus, our results indicate that SCARB2 is essential for EV-A71 infection in RD99 cells but may not be as pivotal in enteroids, despite its absence negatively influencing EV-A71 replication. However, complete KO clones and additional replicates for a statistical analysis are needed to be able to draw conclusions.

SCARB2 does not act as the entry receptor for EV-A71

Upon verifying the importance of SCARB2 for EV-A71 infection, next, we further characterized its role in early steps of the EV-A71 infection cycle. SCARB2 has been extensively shown to act as an uncoating receptor[18], however, it is believed to also have a role as an entry receptor despite its low expression in the plasma membrane. Thus, analysing the potential role of SCARB2 in EV-A71 binding to the cell membrane and internalization was the next step.

As summarized in **Figure 4A**, to analyse SCARB2's role as a binding and internalization receptor, SCARB2^{KO} and WT cells were first inoculated with EV-A71 at 4°C for 1 hour. Low temperatures disrupt Clathrin-mediated endocytosis by inhibiting multiple key components[40], thus, viral particles are only able to bind to the cell surface but not get internalized. Therefore, for the binding assay, after incubation, unbound particles are removed and cell-bound viral particles are collected. For the internalization assay, after removal of unbound viral particles, cultures were incubated at 37°C for an hour to re-activate the endocytosis machinery and enable for viral particle internalization. Unbound and membrane bound particles were then removed, and due to the short incubation time, EV-A71 will not have completed the first replication cycle. Thus, only internalized particles should be present when cells are collected. All samples were then analysed by RT-qPCR to quantify the number of viral RNA copies in the cell.

RD99-WT and RD99-SCARB2^{KO} showed no significant difference in RNA copy numbers of membrane bound EV-A71 viral particles irrespective of the MOI used (**Figure 4B**). Thus, absence of SCARB2 does not impact EV-A71's ability to bind to the cell surface in RD99 cells. To further confirm that SCARB2 does not play a role in EV-A71 viral membrane binding, the binding assay was performed on SCARB2^{KO} enteroid Transwell® models. As shown in **Figure 4C**, no difference in RNA copy numbers for membrane bound EV-A71 was observed when comparing enteroid-WT and enteroid-SCARB2 ^{KO} cells, confirming the data obtained in RD99. Therefore, SCARB2 does not seem to act as a binding receptor, since its absence does not hinder EV-A71 binding efficiency to the cell membrane in neither RD99 nor enteroids. This was further confirmed by an immunostaining of the binding assay, which is shown in

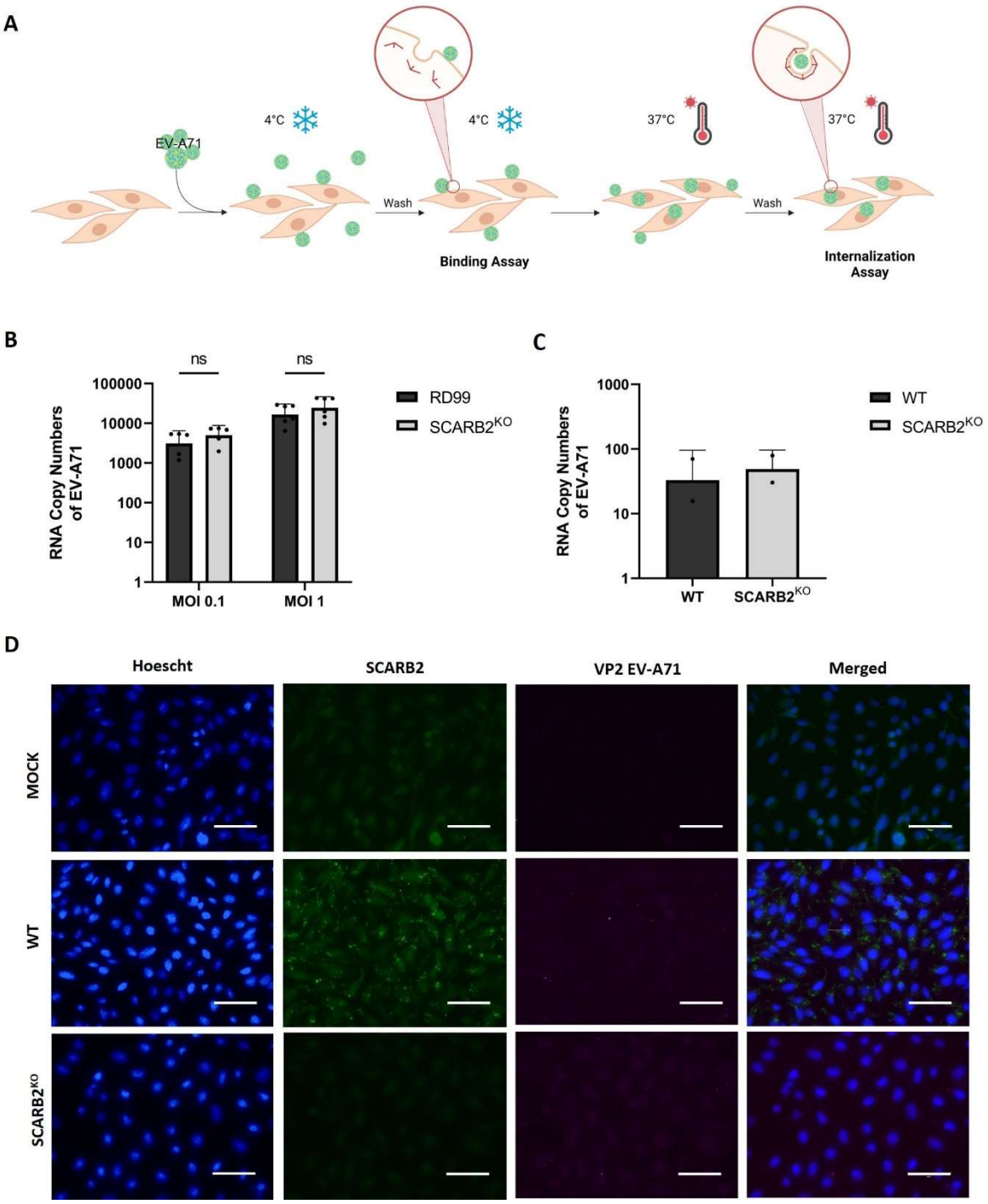

Figure 4. Lack of SCARB2 expression does not affect the ability of EV-A71 to bind to the cell surface. (A) Graphical overview of the binding and internalization assays performed in RD99 and enteroid Transwell® models (Created in Bioredner.com). **(B)** EV-A71 RNA copy numbers of membrane bound viral particles of RD99-WT and RD99-SCARB2^{KO} cell suspension infected with EV-A71 using MOI of 0.1 and 1. **(C)** EV-A71 RNA copy numbers of membrane bound viral particles in Transwell® enteroid-WT and enteroid-SCARB2^{KO} infected with MOI of 1 on the basolateral compartment**. (D)** Immunostaining of the binding assay on RD99-WT and RD99-SCARB2^{KO} cells infected with EV-A71 using an MOI of 5 in IBIDI plates. Cultures were stained with Hoechst (blue), anti-hSCARB2 antibody (green), and anti-VP2-EVA71 (magenta). Scale bars in white represent 50µm.

Figure 4D. RD99-WT and RD99-SCARB2^{KO} showed the presence of membrane bound virus, despite the clear absence of SCARB2 expression in the latter. These results suggest that SCARB2 does not act as an attachment receptor for EV-A71.

Once SCARB2's role as a binding receptor was disproved, we next investigated its involvement in EV-A71 internalization. Similar to the binding assay, no significant difference in EV-A71 RNA copy numbers were found when comparing RD99-WT and RD99-SCARB2^{KO} in neither MOI of 0.1 nor 1 (**Figure 5A**). Furthermore, these results were also confirmed by immunostaining (**Figure 5B**). There was no visible difference in internalized EV-A71 particles between RD99-WT and RD99-SCARB2^{KO} cells. This result suggests that SCARB2 is not involved in the internalization of EV-A71 upon its binding to the cell membrane. To further verify these results, Transwell® enteroid-WT and enteroid-SCARB2^{KO} models were utilized to quantify internalized EV-A71 particles. As shown in **Figure 5C**, there were no differences in internalized EV-A71 RNA copies in the enteroid-SCARB2^{KO} condition when compared to the enteroid-WT. However, experiments must be repeated with additional replicated to statistically confirm that there are no significant differences.

Overall, these results demonstrate SCARB2 does not act as the entry receptor for EV-A71 since it does not aid in viral particle binding to the cell surface, nor is it involved in the internalization of viral particles into the cell.

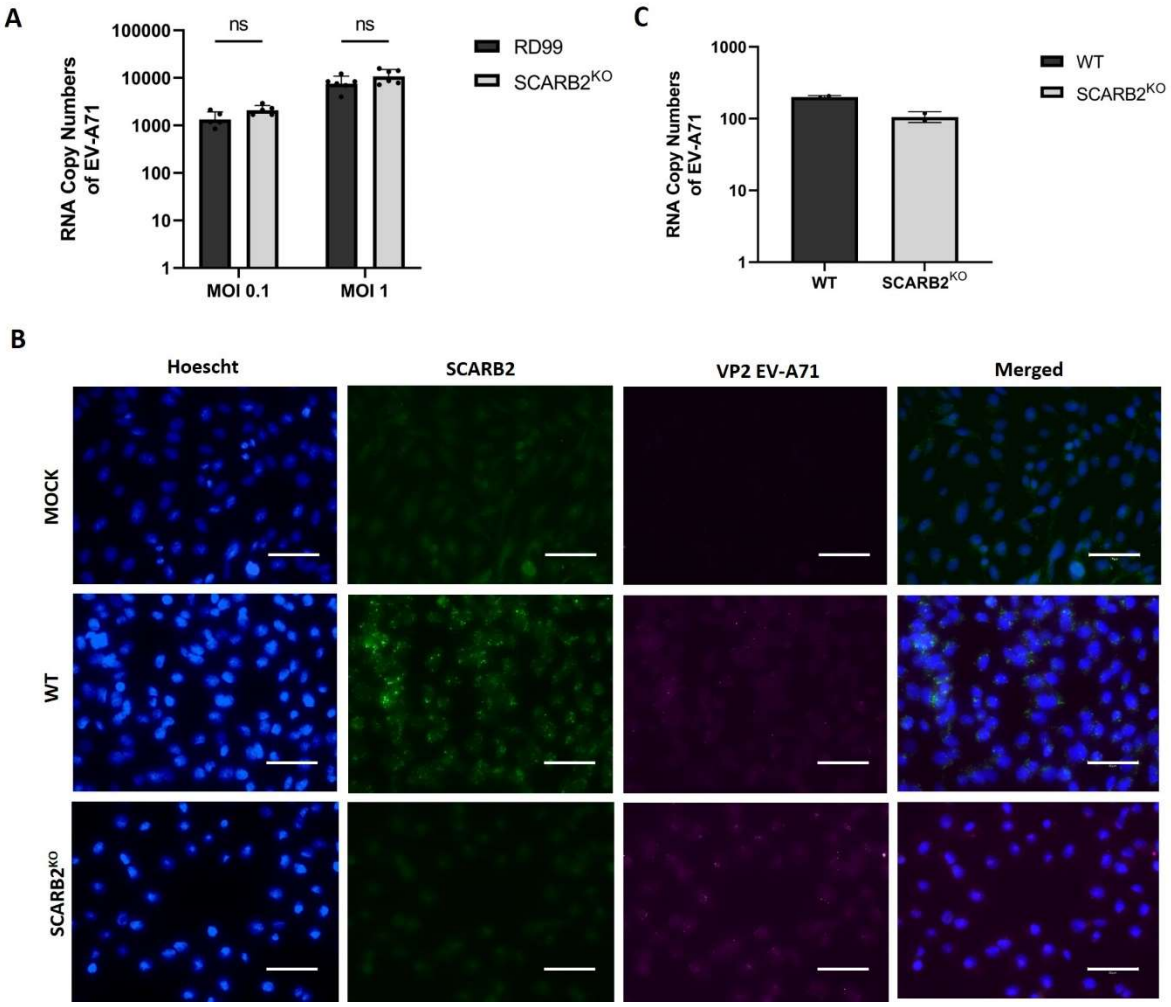

Figure 5. SCARB2 is not involved in internalization of EV-A71 particles. (A) EV-A71 RNA copy numbers of internalized viral particles in RD99-WT and RD99-SCARB2^{KO} cell suspension infected with EV-A71 using MOI of 0.1 and 1. **(B) I**mmunostaining of the internalization assay of RD99-WT and RD99-SCARB2^{KO} cells infected with EV-A71 using an MOI of 5 in IBIDI plates. Cultures were stained with Hoechst (blue), anti-hSCARB2 antibody (green), and anti-VP2-EVA71 (magenta). Scale bars in white represent 50µm. **(C)** EV-A71 RNA copy numbers of internalized viral particles in Transwell® enteroid-WT and enteroid-SCARB2^{KO} cultures infected with MOI of 1 on the basolateral compartment**.**

HSPG2 is not involved in EV-A71 binding nor internalization, and it is not required for infection.

Since SCARB2 was not identified as an entry receptor for EV-A71, other receptors need to fulfil that role for successful EV-A71 infection. A promising group of potential entry receptors are Heparan sulphates (HS) proteins, such as HSPG2, which is highly expressed in the intestine, the primary replication site of EV-A71. Thus, characterizing HSPG2 as a potential entry receptor for EV-A71 was of interest.

To this end, HSPG2 knock-out models on RD99 and enteroids were generated as explained previously (**Figure 2A**). Due to the lack of a working HSPG2 antibody for western blot, the loss of protein expression was not validated. Consequently, the *HSPG2* gene region near the sgRNA sequence of each clonal population was sequenced and compared to the wild type sequence to identify potential indels (nucleotide insertions or deletions). A 1-nucleotide deletion was obtained in the RD99-HSPG2^{KO} clonal population, which leads to a frameshift and appearance of a premature STOP codon (**Figure 6A**). A premature STOP codon suggests the expression of HSPG2 will be interrupted, leading to a truncated dysfunctional peptide which should be rapidly degraded. As shown in **Figure 6B**, a 48-nucleotide deletion was present in the enteroid-HSPG2^{KO} population. This deletion will not result in a frame shift, instead only a part of the amino acid sequence is lost, which could lead to functional loss of HSPG2 due to misfolding. Therefore, we assumed both the RD99 and enteroid HSPG2^{KO} populations nucleotide deletions led to a functional loss of protein expression.

Once HSPG2^{KO} models were generated, to characterize HSPG2 as an entry receptor, first it's role in EV-A71 cell surface binding was characterized. As shown in **Figure 6C**, no significant difference was found between RD99-WT and RD99-HSPG2^{KO} in surface bound viral RNA copy number, irrespective of the MOI tested. Furthermore, EV-A71 particles previously treated with heparin, which blocks EV-A71 binding ability, showed significantly diminished binding when compared to the corresponding MOI of untreated EV-A71. These results suggest heparan sulphates are important for EV-A71 binding to the cell surface, since pre-treatment with heparin blocks their binding ability. Despite this, HSPG2 does not seem to play a role in EV-A71 cell surface binding. To further confirm these findings, a binding assay was also performed on Transwell® enteroid cultures. No difference was seen in RNA copy numbers of bound EV-A71 particles between enteroid-WT and enteroid-HSPG2^{KO} (**Figure 6D**). Altogether, these results demonstrate HSPG2 does not act as a binding receptor for EV-A71.

Once HSPG2 was not identified as a binding receptor, the possibility of HSPG2 being involved in EV-A71 internalization was explored. As shown in **Figure 6E**, RD99-WT and RD99-HSPG2^{KO} cells, at both MOI of 0.1 and 1, showed no significant differences in the number of internalized EV-A71 RNA copy numbers. In the heparin treated conditions, there was fewer internalized viral RNA compared to the non-treated conditions. Thus, in our experiments, HSPG2 did not play a role in EV-A71 internalization nor act as a binding receptor.

Next, we characterized if HSPG2 had an effect on the overall infection capacity of EV-A71 by quantifying the amount of supernatant viral particles overtime. RD99-HSPG2^{KO} cells presented similar levels of CPE as the RD99-WT condition (**Figure 7A**), suggesting HSPG2^{KO} does not hinder EV-A71 cytopathic effect, and hence infectivity. To further confirm this, RT-qPCR on supernatant samples collected 24 hours after initial infection was performed. As shown in **Figure 7B**, the RNA copy numbers of EV-A71 in RD99-HSPG2^{KO} did not significantly differ from RD99-WT EV-A71 copy numbers in all MOI tested. Moreover, heparin pre-treatment of EV-A71 seemed to significantly decrease the viral RNA copies when compared to the untreated conditions, further confirming the role of heparan sulphates

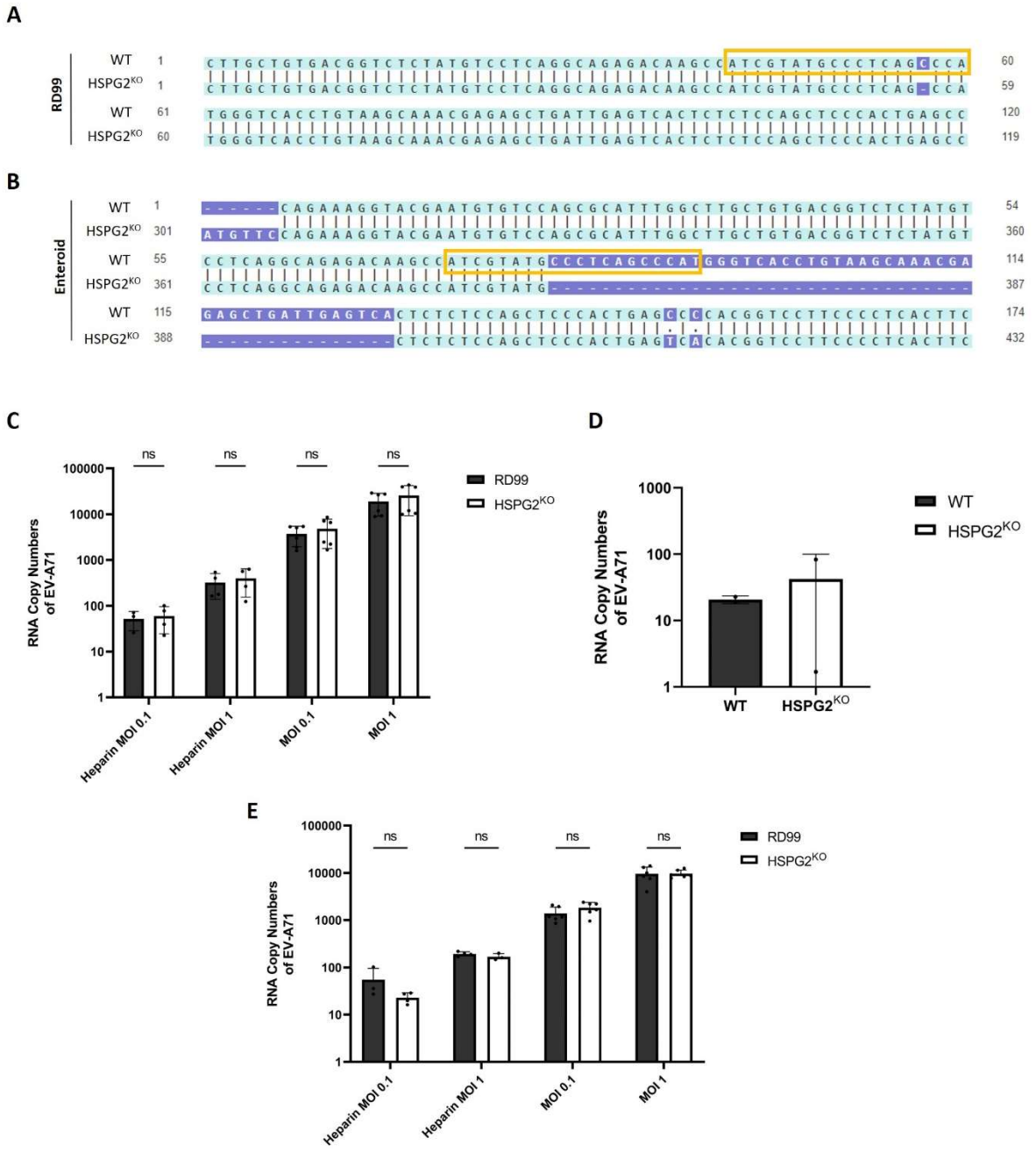

Figure 6. HSPG2 is not involved in the internalization and binding of EV-A71 particles. Alignment of nucleic acid sequences of **(A)** RD99-WT with clonal RD99-HSPG2^{KO} cells and **(B)** enteroid-WT and clonal enteroid-HSPG2^{KO} cells. The sgRNA target sequence is highlighted in yellow while mismatches and indels found are in purple. **(C)** EV-A71 RNA copy number of membrane bound viral particles in RD99-WT and RD99-HSPG2^{KO} cells infected with heparin-treated and un-treated EV-A71 using MOI of 0.1 and 1. **(D)** EV-A71 RNA copy numbers of membrane bound viral particles in Transwell® enteroid-WT and enteroid-HSPG2^{KO} cultures infected with a MOI of 1 on the basolateral compartment**. (E)** EV-A71 RNA copy numbers of internalized viral particles in RD99-WT and RD99-HSPG2^{KO} cells infected with heparin-treated and un-treated EV-A71 using a MOI of 0.1 and 1.

in EV-A71 infection. Finally, HSPG2's role on EV-A71 infection was analysed in Transwell® enteroid models,

to consolidate the results found on RD99. After 24-, 48- and 72-hours post EV-A71 infection, similar RNA copy numbers were obtained between enteroid-WT and enteroid-HSPG2^{KO}, confirming HSPG2 is not involved in EV-A71 infection (**Figure 7C**). Interestingly, it seems a higher RNA copy number of EV-A71 is present in enteroid-HSPG2^{KO} condition 12 hours post infection when compared to enteroid-WT. This suggests HSPG2 absence might facilitate initial binding to other cell surface proteins, and hence replication.

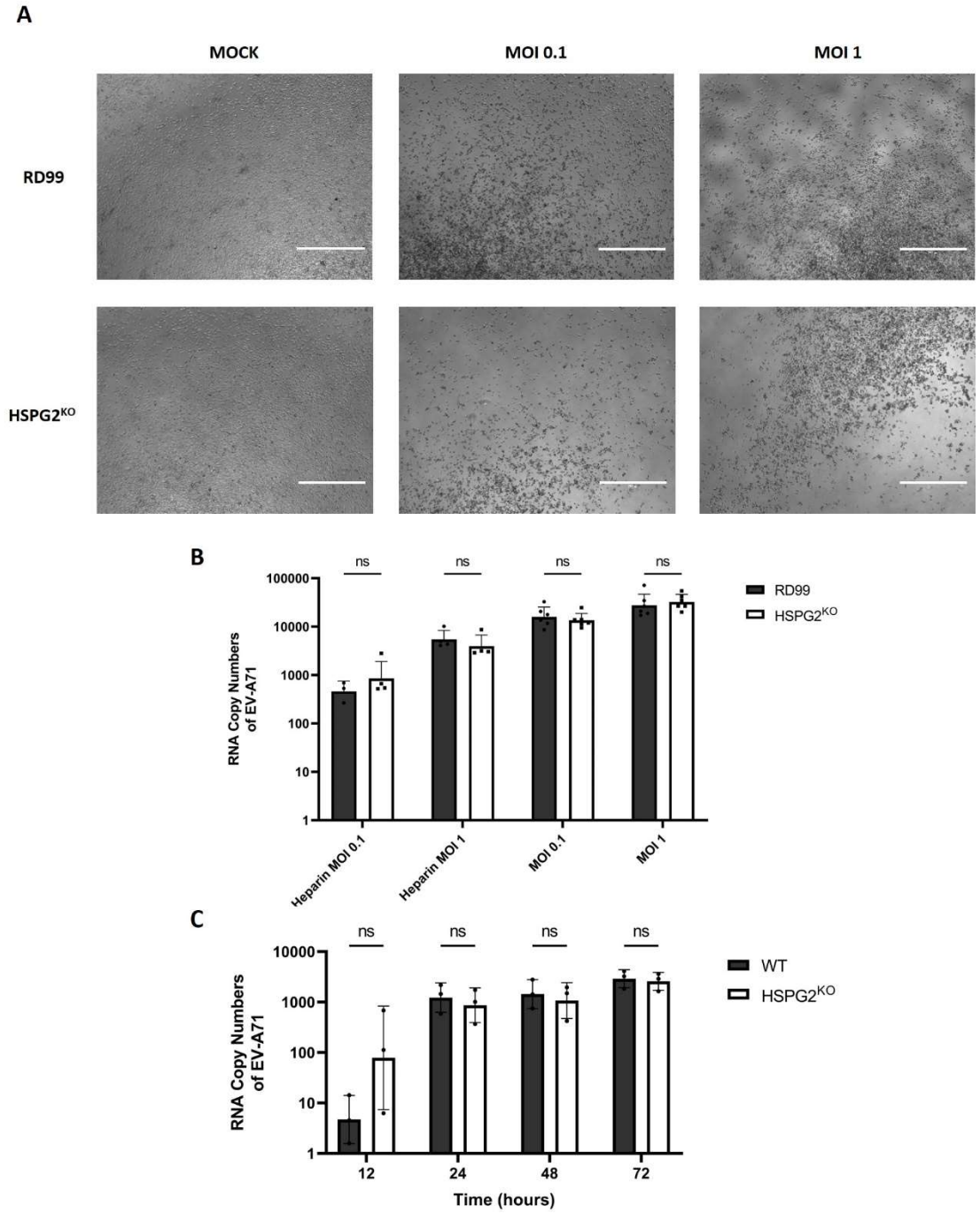

Figure 7. EV-A71 infection is independent of HSPG2. (A) Bright field images depicting cytopathic effect (CPE) induced by EV-A71 infection of RD99-WT and RD99-HSPG2^{KO} clonal population using MOI of 0.1 and 1. Scale bars in white represent 750µm. **(B)** Viral RNA copy numbers of EV-A71 of RD99-WT and RD99-HSPG2^{KO} supernatant samples after 24h of heparin treated and un-treated EV-A71 infection at an MOI of 0.1 and 1. **(C)** Viral RNA copy numbers of EV-A71 in enteroid-WT and enteroid-HSPG2^{KO} supernatant samples collected from the apical compartment of the Transwell® 24-, 48- and 72-hours post infection. Transwell® cultures were infected with an MOI of 1 through the basolateral compartment.

Overall, these results suggest HSPG2 is not needed for EV-A71 infection and does not act as an entry receptor, since it's not involved in cell surface binding nor internalization. Furthermore, HSPG2^{KO} did not affect the replication capacity of EV-A71 after infection in either RD99 or enteroids.

DISCUSSION

Viral entry into a host cell is the first and a crucial step for viral infection and replication. Thus, a complete understanding of the mechanisms and receptors involved is of outmost importance to prevent entry of viral particles and fight against infection. In this study, we generated *SCARB2* and *HSPG2* knock-outs in cell lines and enteroids to characterize the role of these proteins as potential entry receptors in EV-A71 infection, further contributing to the understanding of EV-A71's elusive entry mechanism.

SCARB2 was chosen as the first protein of interest as this is the most studied protein in the context of EV-A71 infection. SCARB2's major role in EV-A71 infection is known to be as an uncoating receptor in the lysosome, which has been studied extensively over the years[18,19,41]. Moreover, SCARB2 has also been shown to act as an entry receptor for EV-A71, a role which is also largely accepted in the field. For instance, Yamayoshi et al., 2013[20] and Lin et al., 2012[21] showed that SCARB2 acts as an attachment receptor for EV-A71. Furthermore, Yamayoshi et al. also showed SCARB2's role in internalization of EV-A71 particles in cell line models. Multiple other studies, also characterized the mechanism of binding of SCARB2 with EV-A71 particles at the molecular and biological level, all suggesting SCARB2's role as an attachment receptor[18,42–44]. However, due to SCARB2's scarce expression at the cell membrane[16], we hypothesized that SCARB2 is unlikely to act as an attachment receptor and consequently, unlikely to be critical for internalization.

To validate this hypothesis, we generated SCARB2^{KO} RD99 cells and enteroids which were validated by western blotting. RD99 cells showed complete loss of SCARB2 expression and the lack of SCARB2 expression was confirmed by immunostaining. In line with previous findings[45–47], we observed that SCARB2 plays a pivotal role in EV-A71 infection. SCARB2^{KO} in RD99 strongly hindered EV-A71 infection and no CPE was observed in the KO lines. As cells lines are highly variable and often reproducibility of results using the same lines is lacking, we aimed to validate our findings using physiologically relevant enteroid models. To this end, we generated enteroid SCABR2^{KO} lines. A similar effect to RD99 cells was also observed in the enteroid KO lines. However, the effect of SCARB2^{KO} in RD99 and in enteroids was not comparable, since a 100-fold decrease in viral copy numbers was observed in RD99 compared to a 10-fold decrease in enteroids. This could potentially be explained due to a partial knock-out in the enteroid lines. The enteroid SCARB2^{KO} clonal population showed a very faint band, thus, only a partial loss of SCARB2 expression was obtained. This suggests that the enteroid clonal population was not composed of only KO cells, but a small percentage of the population was likely wild type. Alternatively, the deletions in the *SCARB2* gene only partially affect protein expression or the deletions were hemizygous. Sequencing of the KO lines will be indicative of the regions and extent of the KO in the enteroid population. Moreover, generation of new enteroid lines completely lacking SCARB2 expression and inclusion of additional replicates (enteroids derived from multiple donors) should be performed to confirm these findings.

After confirming that SCARB2 was critical for EV-A71 infection, we then evaluated its role as an entry receptor. We observed that the KO of SCARB2 does not have a significant effect in the binding nor internalization efficiency of EV-A71 particles in either RD99 or enteroid SCARB2^{KO} clonal populations when compared to their wild type counterparts. This suggests that SCARB2 was not necessary in the attachment of EV-A71 particles to the cell membrane, nor played a role in the internalization of viral particles. To further consolidate these findings, we visualized via immunostaining the bound and

internalized EV-A71 particles in wild type and SCARB2^{KO} RD99 cells. As expected, there was no detectable difference of bound or internalized EV-A71 particles when SCARB2 was present or absent. Therefore, in our study SCARB2 was only a critical factor post-internalization and most likely to be involved in uncoating rather than entry.

Although previous studies exploring the role of SCARB2 on EV-A71 entry are contradictory to our findings, these studies are based on overexpression of human SCARB2 in different cell lines[20,21]. However, genetic complementation of heterologous proteins has its drawbacks and may result in the abnormal presence of expressed proteins in the plasma membrane[48–50]. This overexpression can also influence the biological function and interaction with other factors due to its potential concentration-dependent nature[51]. Furthermore, SCARB2 EV-A71 binding studies were done with soluble hSCARB2 protein to assess the molecular mechanisms of the binding. Thus, although they do indeed confirm SCARB2 can bind to EV-A71, it does not prove the interaction happens in the cell membrane nor that EV-A71 preferentially binds SCARB2. Most likely, upon endolysosome formation, EV-A71 binds to SCARB2 in the lysosomal microenvironment, allowing the uncoating of the viral particle in low pH conditions. Hence, our findings in cell lines and enteroids, should provide stronger indication of the non-involvement of SCARB2 in the binding and internalization of EV-A71, and thus, disproving its role as an entry receptor. This is in line with a more recent study, which used CRISPR-Cas9 KOs on HeLa and RD99 cells[52].

As our data demonstrated that SCARB2 is not an entry receptor for EV-A71, we sought to assess other proteins that have been suggested as entry or binding receptors. To our knowledge, a total of 12 proteins have been suggested to play a role in EV-A71 entry[53], with a large number of studies on PSGL-1[20], and HSPGs[22]. Although PSGL-1 has been shown to be involved in EV-A71 infection[54], it's expression in the intestine epithelium, the main replication site of EV-A71, is scarce when compared to the highly expressed HSPGs[25,55]. Several studies have already shown the importance of heparan sulphates (HS), negatively charged polysaccharides which are attached to a core protein forming HSPGs, in EV-A71 attachment[22,56]. Given the basolateral polarity of EV-A71 infection in our cultures, we hypothesized that HSPG2 may play a role in entry as it is primarily secreted in the basement membrane of the intestine[57]. Thus, we set to characterize the role of HSPG2, as an entry receptor for EV-A71[25].

However, our results showed that HSPG2 does not play a role in any steps of EV-A71 infection in both cells lines and enteroids. First, HSPG2 KO did not affect the CPE induced by EV-A71 infection nor the overall copy numbers. Second, HSPG2 KO did not influence internalization as no significant differences were observed between KO and wild type cells. Finally, the binding capacity of EV-A71 to target cells was not affected by HSPG2 KO. However, as demonstrated previously by us and others, EV-A71 is capable of binding negatively charged HS as pre-treatment with soluble heparin inhibits infection. Thus, while other HSPGs may be involved in EV-A71 infection, our study indicates that HSPG2 may not be necessary.

A key limitation of our findings is that the HSPG2 KO in RD99 and enteroid populations could not be confirmed by a western blot due to a lack of a suitable antibody, thus only sequencing was used as validation. Our sequencing data showed a single nucleotide deletion in RD99 cells led to a premature STOP codon. For the enteroid population, a 48-nucleotide deletion in the HSPG2 gene was obtained, which remained in frame and therefore, does not guarantee a functional loss. Nevertheless, given the size of the deletion, we assumed there was a significant defect in HSPG2 translation. However, our results must be confirmed in knockouts with frameshift mutations and loss of protein expression. As an alternative to western blot, ELISA could be used to validate the loss of HSPG2 protein expression.

HSPGs have been identified as important attachment receptors for viruses due to the presence of sulphate groups in the HS chains which results in an overall negative charge. As the EV-A71 viral capsid contains positively charged amino acids, electrostatic interactions can drive EV-A71 to bind to HSPGs as attachment receptors[22,56]. However, the negative charge on HSPGs is not due to the polysaccharide composition but rather due to post-translational modification that introduce sulphate groups. In accordance, Guo et al. 2022, recently reported a positive correlation between the levels of host cell sulfation and EV-A71 infection efficiency[52]. Specifically, they identified SLC35B2, a Golgi apparatus sulfate 3'-phosphoadenosine-5'-phosphosulfate (PAPS) transporter, as a key host factor indirectly facilitating EV-A71 infection. SLC35B2-mediated transport of PAPs into the Golgi modulates sulfation on HSPGs and SCARB2. These added sulphate groups facilitated the electrostatic interaction of these proteins with EV-A71. However, this study was performed using cell lines and verification with enteroids will confirm the role of host protein sulfation for EV-A71 entry while also explaining the inhibition by HS treatment.

To conclude, we have demonstrated the crucial role of SCARB2 in EV-A71 infection but contrary to previous reports, we demonstrate that the role is limited to post-internalization. Furthermore, we found HSPG2 is not involved in EV-A71 infection nor act as an entry receptor, despite being composed of heparan sulphate chains. Our findings further shed light on specific host proteins in the early stages of EV-A71 infections and crucially, for the first time, in a physiologically relevant model of the human intestine. Further optimization and validation of our results in the enteroid models will be valuable for unravelling EV-A71 pathogenesis.

LAYMAN'S SUMMARY:

Enterovirus A71 (EV-A71) is a non-enveloped, positive single-stranded RNA virus belonging to the *Picornaviridae* family, which is considered a major public health concern due to recent global outbreaks[1–3]. EV-A71 is one of the main causative agents of hand, foot and mouth diseases (HFMD)[5] and it can cause illness in multiple organs, such as the gastrointestinal and respiratory tract[6]. Most worrisome however, is EV-A71's ability to infect the central nervous system (CNS)[9]. It is considered to be the most neurotoxic enterovirus[12] due to potential life-threatening consequences in young children. Despite this, the entry mechanism EV-A71 utilizes to enter the host cell and initiate infection remains elusive. Thus, fully understanding the factors involved in viral entry in the primary replication site, the gastrointestinal tract, is a crucial step towards combating EV-A71 infection.

Multiple receptors have been shown to be involved in EV-A71 infection over the years, such as SCARB2[15] and HSPGs[22]. SCARB2, a lysosomal protein, is believed to play a role in uncoating the viral capsid[18], as well as act as an entry receptor[20]. However, due to SCARB2's low expression in the cell membrane[16], its role as an entry receptor is unlikely. Thus, other factors, such as HSPG2, might fulfil this role. Most studies on EV-A71 entry have been performed in cell lines, models which present multiple crucial limitations[29,30,32]. To overcome these limitations, enteroids, which are human 3D tissue cultures mimicking the function and structure of the intestine[35], are promising tools for the study of EV-A71 infection. Therefore, in this study we aimed to characterize the role of SCARB2 and HSPG2 in EV-A71 infection using more physiologically relevant models, enteroids, as well as cell lines. To do so, we utilized CRISPR-Cas9 technology, to knock-out SCARB2 and HSPG2 in these models, which allows for the loss of expression of these proteins.

Here, we showed SCARB2 plays a pivotal role in EV-A71 infection, since loss of SCARB2 expression significantly hindered EV-A71 infection in both cell lines and enteroids. Furthermore, SCARB2 loss did not affect the binding ability of EV-A71 to the cell membrane, nor did it hinder the internalization of viral particles inside the cell. Thus, our study presents SCARB2 as an essential factor for EV-A71

infection only post-internalization, disproving SCARB2's role as an entry receptor demonstrated in previous reports. Following these findings, we sought to assess another protein which was suggested to be involved in EV-A71 entry, HSPG2. Our findings showed HSPG2 loss did not impact EV-A71 binding to the cell membrane nor internalization into the cell, hence HSPG2 is not an entry receptor of EV-A71. Furthermore, EV-A71 infection was not hindered after loss of HSPG2 expression in neither cell lines nor enteroids. Thus, in our study HSPG2 did not play a role in any steps of EV-A71 infection.

Overall, we have demonstrated the crucial role of SCARB2 in EV-A71 infection and showed its role is limited to post-internalization stages. Furthermore, we showed EV-A71 infection is independent of HSPG2. These findings, shed a light on specific host proteins in the early stages of EV-A71 infection in physiologically relevant models. Finally, it stresses the need to further characterize EV-A71's entry pathway in order to fully understand EV-A71 viral pathogenesis.

References:

1. Wang J, Hu Y, Zheng M. Enterovirus A71 antivirals: Past, present, and future. *Acta Pharmaceutica Sinica B*. 2022;12(4):1542-1566. doi:10.1016/j.apsb.2021.08.017

2. Autore G, Bernardi L, Perrone S, Esposito S. Update on Viral Infections Involving the Central Nervous System in Pediatric Patients. *Children (Basel)*. 2021;8(9):782. doi:10.3390/children8090782

3. de Ceano-Vivas M, García ML, Velázquez A, et al. Neurodevelopmental Outcomes of Infants Younger Than 90 Days Old Following Enterovirus and Parechovirus Infections of the Central Nervous System. *Frontiers in Pediatrics*. 2021;9. Accessed December 7, 2022. https://www.frontiersin.org/articles/10.3389/fped.2021.719119

4. Puenpa J, Wanlapakorn N, Vongpunsawad S, Poovorawan Y. The History of Enterovirus A71 Outbreaks and Molecular Epidemiology in the Asia-Pacific Region. *Journal of Biomedical Science*. 2019;26(1):75. doi:10.1186/s12929-019-0573-2

5. Nayak G, Bhuyan SK, Bhuyan R, Sahu A, Kar D, Kuanar A. Global emergence of Enterovirus 71: a systematic review. *Beni Suef Univ J Basic Appl Sci*. 2022;11(1):78. doi:10.1186/s43088-022-00258-4

6. de Crom SCM, Rossen JWA, van Furth AM, Obihara CC. Enterovirus and parechovirus infection in children: a brief overview. *Eur J Pediatr*. 2016;175:1023-1029. doi:10.1007/s00431-016-2725-7

7. Dong Y, Liu J, Lu N, Zhang C. Enterovirus 71 Antagonizes Antiviral Effects of Type III Interferon and Evades the Clearance of Intestinal Intraepithelial Lymphocytes. *Frontiers in Microbiology*. 2022;12. Accessed June 11, 2023. https://www.frontiersin.org/articles/10.3389/fmicb.2021.806084

8. Li H guo, Lao Q. The pulmonary complications associated with EV71-infected hand–foot–mouth disease. *Radiology of Infectious Diseases*. 2017;4(4):137-142. doi:10.1016/j.jrid.2017.01.001

9. Lee KY. Enterovirus 71 infection and neurological complications. *Korean J Pediatr*. 2016;59(10):395-401. doi:10.3345/kjp.2016.59.10.395

10. Gu J, Zhao Y, Wu J, et al. Enterovirus-71 utilizes small extracellular vesicles to cross the blood–brain barrier for infecting the central nervous system via transcytosis. *Journal of Medical Virology*. 2023;95(1). doi:10.1002/jmv.28120

11. Aubart M, Gitiaux C, Roux CJ, et al. Severe Acute Flaccid Myelitis Associated With Enterovirus in Children: Two Phenotypes for Two Evolution Profiles? *Front Neurol*. 2020;11:343. doi:10.3389/fneur.2020.00343

12. Enterovirus 71. Accessed June 18, 2023. https://www.who.int/teams/health-product-policy-and-standards/standards-and-specifications/vaccine-standardization/enterovirus-71

13. Wells AI, Coyne CB. Enteroviruses: A Gut-Wrenching Game of Entry, Detection, and Evasion. *Viruses*. 2019;11(5):460. doi:10.3390/v11050460

14. Yamayoshi S, Iizuka S, Yamashita T, et al. Human SCARB2-Dependent Infection by Coxsackievirus A7, A14, and A16 and Enterovirus 71. *Journal of Virology*. 2012;86(10):5686-5696. doi:10.1128/JVI.00020-12

15. Tang Q, Xu Z, Zhang F, et al. Identification of a novel binding inhibitor that blocks the interaction between hSCARB2 and VP1 of enterovirus 71. *Cell Insight*. 2022;1(2):100016. doi:10.1016/j.cellin.2022.100016

16. Kobayashi K, Koike S. Cellular receptors for enterovirus A71. *Journal of Biomedical Science*. 2020;27(1):23. doi:10.1186/s12929-020-0615-9

17. Blanz J, Groth J, Zachos C, Wehling C, Saftig P, Schwake M. Disease-causing mutations within the lysosomal integral membrane protein type 2 (LIMP-2) reveal the nature of binding to its ligand β-glucocerebrosidase. *Human Molecular Genetics*. 2010;19(4):563-572. doi:10.1093/hmg/ddp523

18. Dang M, Wang X, Wang Q, et al. Molecular mechanism of SCARB2-mediated attachment and uncoating of EV71. *Protein Cell*. 2014;5(9):692-703. doi:10.1007/s13238-014-0087-3

19. Chen P, Zilin S, Yonghe Q, et al. Molecular Determinants of Enterovirus 71 Viral Entry: cleft around GLN-172 on VP1 protein interacts with variable region on scavenge receptor B 2. *The Journal of biological chemistry*. 2012;287:6406-6420. doi:10.1074/jbc.M111.301622

20. Yamayoshi S, Ohka S, Fujii K, Koike S. Functional Comparison of SCARB2 and PSGL1 as Receptors for Enterovirus 71. *Journal of Virology*. 2013;87(6):3335-3347. doi:10.1128/JVI.02070-12

21. Lin YW, Lin HY, Tsou YL, et al. Human SCARB2-Mediated Entry and Endocytosis of EV71. *PLOS ONE*. 2012;7(1):e30507. doi:10.1371/journal.pone.0030507

22. Tan CW, Poh CL, Sam IC, Chan YF. Enterovirus 71 Uses Cell Surface Heparan Sulfate Glycosaminoglycan as an Attachment Receptor. *Journal of Virology*. 2013;87(1):611-620. doi:10.1128/JVI.02226-12

23. Nishimura Y, Shimojima M, Tano Y, Miyamura T, Wakita T, Shimizu H. Human P-selectin glycoprotein ligand-1 is a functional receptor for enterovirus 71. *Nat Med*. 2009;15(7):794-797. doi:10.1038/nm.1961

24. Yang SL, Chou YT, Wu CN, Ho MS. Annexin II Binds to Capsid Protein VP1 of Enterovirus 71 and Enhances Viral Infectivity. *Journal of Virology*. 2011;85(22):11809-11820. doi:10.1128/JVI.00297-11

25. Tissue expression of HSPG2 - Summary - The Human Protein Atlas. Accessed December 13, 2022. https://www.proteinatlas.org/ENSG00000142798-HSPG2/tissue

26. Martinez JR, Dhawan A, Farach-Carson MC. Modular Proteoglycan Perlecan/HSPG2: Mutations, Phenotypes, and Functions. *Genes (Basel)*. 2018;9(11):556. doi:10.3390/genes9110556

27. Cagno V, Tseligka ED, Jones ST, Tapparel C. Heparan Sulfate Proteoglycans and Viral Attachment: True Receptors or Adaptation Bias? *Viruses*. 2019;11(7):596. doi:10.3390/v11070596

28. Gillet JP, Varma S, Gottesman MM. The Clinical Relevance of Cancer Cell Lines. *J Natl Cancer Inst*. 2013;105(7):452-458. doi:10.1093/jnci/djt007

29. Hynds RE, Vladimirou E, Janes SM. The secret lives of cancer cell lines. *Dis Model Mech*. 2018;11(11):dmm037366. doi:10.1242/dmm.037366

30. Lawko N, Plaskasovitis C, Stokes C, et al. 3D Tissue Models as an Effective Tool for Studying Viruses and Vaccine Development. *Frontiers in Materials*. 2021;8. Accessed December 14, 2022. https://www.frontiersin.org/articles/10.3389/fmats.2021.631373

31. Aknouch I, García-Rodríguez I, Giugliano F, et al. *Amino Acid Variation at VP1-145 of Enterovirus A71 Determines the Viral Infectivity and Receptor Usage in a Primary Human Intestinal Model*. Zenodo; 2022. doi:10.5281/zenodo.5843780

32. Mouriaux F, Zaniolo K, Bergeron MA, et al. Effects of Long-term Serial Passaging on the Characteristics and Properties of Cell Lines Derived From Uveal Melanoma Primary Tumors. *Investigative Ophthalmology & Visual Science*. 2016;57(13):5288-5301. doi:10.1167/iovs.16-19317

33. Ben-David U, Siranosian B, Ha G, et al. Genetic and transcriptional evolution alters cancer cell line drug response. *Nature*. 2018;560(7718):325-330. doi:10.1038/s41586-018-0409-3

34. Sridhar A, Simmini S, Ribeiro CMS, et al. A Perspective on Organoids for Virology Research. *Viruses*. 2020;12(11):1341. doi:10.3390/v12111341

35. Sang Y, Miller LC, Nelli RK, Giménez-Lirola LG. Harness Organoid Models for Virological Studies in Animals: A Cross-Species Perspective. *Frontiers in Microbiology*. 2021;12. Accessed December 14, 2022. https://www.frontiersin.org/articles/10.3389/fmicb.2021.725074

36. Sato T, Vries RG, Snippert HJ, et al. Single Lgr5 stem cells build crypt-villus structures in vitro without a mesenchymal niche. *Nature*. 2009;459(7244):262-265. doi:10.1038/nature07935

37. García-Rodríguez I, Sridhar A, Pajkrt D, Wolthers KC. Put Some Guts into It: Intestinal Organoid Models to Study Viral Infection. *Viruses*. 2020;12(11):1288. doi:10.3390/v12111288

38. REED LJ, MUENCH H. A SIMPLE METHOD OF ESTIMATING FIFTY PER CENT ENDPOINTS12. *American Journal of Epidemiology*. 1938;27(3):493-497. doi:10.1093/oxfordjournals.aje.a118408

39. Roodsant T, Navis M, Aknouch I, et al. A Human 2D Primary Organoid-Derived Epithelial Monolayer Model to Study Host-Pathogen Interaction in the Small Intestine. *Frontiers in Cellular and Infection Microbiology*. 2020;10. Accessed June 19, 2023. https://www.frontiersin.org/articles/10.3389/fcimb.2020.00272

40. Chanaday NL, Kavalali ET. Time course and temperature dependence of synaptic vesicle endocytosis. *FEBS Lett*. 2018;592(21):3606-3614. doi:10.1002/1873-3468.13268

41. Ohka S, Tan SH, Ishiyama E, et al. The uncoating of EV71 in mature late endosomes requires CD-M6PR. *Biol Open*. 2022;11(9):bio059469. doi:10.1242/bio.059469

42. Yamayoshi S, Yamashita Y, Li J, et al. Scavenger receptor B2 is a cellular receptor for enterovirus 71. *Nat Med*. 2009;15(7):798-801. doi:10.1038/nm.1992

43. Zhou D, Zhao Y, Kotecha A, et al. Unexpected mode of engagement between enterovirus 71 and its receptor SCARB2. *Nat Microbiol*. 2019;4(3):414-419. doi:10.1038/s41564-018-0319-z

44. Yamayoshi S, Koike S. Identification of a Human SCARB2 Region That Is Important for Enterovirus 71 Binding and Infection ▿. *J Virol*. 2011;85(10):4937-4946. doi:10.1128/JVI.02358-10

45. Zhang X, Yang P, Wang N, et al. The binding of a monoclonal antibody to the apical region of SCARB2 blocks EV71 infection. *Protein Cell*. 2017;8(8):590-600. doi:10.1007/s13238-017-0405-7

46. Jin Y, Sun T, Zhou G, et al. Pathogenesis Study of Enterovirus 71 Using a Novel Human SCARB2 Knock-In Mouse Model. *mSphere*. 2021;6(2):10.1128/msphere.01048-20. doi:10.1128/msphere.01048-20

47. Li X, Fan P, Jin J, et al. Establishment of cell lines with increased susceptibility to EV71/CA16 by stable overexpression of SCARB2. *Virology Journal*. 2013;10(1):250. doi:10.1186/1743-422X-10-250

48. Prelich G. Gene Overexpression: Uses, Mechanisms, and Interpretation. *Genetics*. 2012;190(3):841-854. doi:10.1534/genetics.111.136911

49. Roux A, Beloin C, Ghigo JM. Combined Inactivation and Expression Strategy To Study Gene Function under Physiological Conditions: Application to Identification of New Escherichia coli Adhesins. *J Bacteriol*. 2005;187(3):1001-1013. doi:10.1128/JB.187.3.1001-1013.2005

50. Simm D, Popova B, Braus G, Waack S, Kollmar M. Design of typical genes for heterologous gene expression. *Scientific Reports*. 2022;12. doi:10.1038/s41598-022-13089-1

51. Kramer E. A stranger in a strange land: the utility and interpretation of heterologous expression. *Frontiers in Plant Science*. 2015;6. Accessed June 27, 2023. https://www.frontiersin.org/articles/10.3389/fpls.2015.00734

52. Guo D, Yu X, Wang D, et al. SLC35B2 Acts in a Dual Role in the Host Sulfation Required for EV71 Infection. *J Virol*. 96(9):e02042-21. doi:10.1128/jvi.02042-21

53. Hu K, Onintsoa Diarimalala R, Yao C, Li H, Wei Y. EV-A71 Mechanism of Entry: Receptors/Co-Receptors, Related Pathways and Inhibitors. *Viruses*. 2023;15(3):785. doi:10.3390/v15030785

54. Nishimura Y, Lee H, Hafenstein S, et al. Enterovirus 71 binding to PSGL-1 on leukocytes: VP1-145 acts as a molecular switch to control receptor interaction. *PLoS Pathog*. 2013;9(7):e1003511. doi:10.1371/journal.ppat.1003511

55. Jiao XY, Guo L, Huang DY, Chang XL, Qiu QC. Distribution of EV71 receptors SCARB2 and PSGL-1 in human tissues. *Virus Research*. 2014;190:40-52. doi:10.1016/j.virusres.2014.05.007

56. Tee HK, Tan CW, Yogarajah T, et al. Electrostatic interactions at the five-fold axis alter heparin-binding phenotype and drive enterovirus A71 virulence in mice. *PLoS Pathog*. 2019;15(11):e1007863. doi:10.1371/journal.ppat.1007863

57. Yamamoto S, Nakase H, Matsuura M, et al. Heparan sulfate on intestinal epithelial cells plays a critical role in intestinal crypt homeostasis via Wnt/β-catenin signaling. *Am J Physiol Gastrointest Liver Physiol*. 2013;305(3):G241-G249. doi:10.1152/ajpgi.00480.2012